NASA Contractor Report 202347

Characterization and Demonstrations of Laser-Induced Incandescence in Both Normal and Low-Gravity

Randall L. Vander Wal
NYMA, Inc.
Brook Park, Ohio

May 1997

Prepared for
Lewis Research Center
Under Contract NAS3–27186

National Aeronautics and
Space Administration

Characterization and Demonstrations of Laser-Induced Incandescence in Both Normal and Low Gravity

R.L. Vander Wal
Nyma@NASA-Lewis
M.S. 110-3
21000 Brookpark Rd.
Cleveland, OH 44135

Ph. (216) 433-9065
Fax (216) 433-3793
email: randy@rvander.lerc.nasa.gov

Abstract

Knowledge of soot volume fraction is important to a wide range of combustion studies in microgravity. Laser-induced incandescence (LII) offers high sensitivity, high temporal and spatial resolution in addition to geometric versatility for real-time determination of soot volume fraction. Implementation of LII into the 2.2 sec drop tower at The NASA-Lewis Research Center along with system characterization is described. Absolute soot volume fraction measurements are presented for laminar and turbulent gas-jet flames in microgravity to illustrate the capabilities of LII in microgravity. Comparison between LII radial intensity profiles with soot volume fraction profiles determined through a full-field light extinction technique (Greenberg, P.S. and Ku, J.C., Comb. and Flame 108:227-230 (1997)) are also reported validating the accuracy of LII for soot volume fraction measurements in a microgravity environment.

Introduction

Determination of soot volume fraction (f_v) is important due to the wide range of combustion processes in which soot is found ranging from diffusion to premixed flames, laminar to turbulent processes and homogeneous to heterogeneous combustion. In addition to representing incomplete combustion and an unwanted pollutant when emitted from flames, the presence of soot also affects other physical and chemical properties of combustion. Low soot loadings (<1 ppm) within flames can make a contribution comparable to gaseous radiative emission [1]. High soot loadings can cause the radiative heat release to be greater than 30% of the total enthalpy of combustion [2]. Radiative heat loss from the flame will lower the flame temperature which in turn alters the chemical kinetics [3]. The presence of soot also alters the oxidation rates of combustion intermediates apart from a temperature effect. Soot acts as a sink for key CO oxidizers such as OH and O causing increased CO emission levels from flames [4]. The radiative emission from a flame can also affect its propagation. Liquid fuel vaporization and solid fuel pyrolysis reactions are the first steps in flame spread along liquids and solids and are critically dependent upon soot radiation [5,6].

Microgravity offers unique opportunities for studying both soot growth and the effect of soot radiation upon flame structure and spread [7]. Spatial scales and residence time scales are greatly extended in 0-g facilitating soot growth studies. With the varied geometries, short duration microgravity test times and time-varying processes, there is demand for measurement of f_v with high spatial plus temporal resolution and sensitivity.

LII has advanced f_v measurements in many 1-g combustion processes. By virtue of its high sensitivity, geometric versatility and temporal capability, LII offers many advantages compared to traditional techniques for measurement of f_v as demonstrated by application of LII to internal combustion engines [8,9], laminar [10-16] and turbulent gas-jet diffusion flames [14,17], rich premixed flames [11] and droplet combustion [18]. Since the LII signal can be created with a 10 ns duration laser pulse and signal collection in an imaging mode can be achieved within the same timescale, the technique possesses high temporal capability. The spatial resolution is determined by the imaging optics used and laser sheet thickness and with commercially available lenses and CCD arrays, can be better than 0.1 mm The geometric versatility of LII arises from the ability to orient a laser sheet at various angles relative to the detection (imaging) axis and combustion process. With suitable spectral filtering or use of excitation wavelengths not detected by common photocathode materials, heterogeneous combustion processes do not present scattered laser light interferences.

In contrast to the advantages offered to combustion studies by a microgravity environment, advanced diagnostics, specifically pulsed laser diagnostics have been limited due to equipment size, weight and power limitations in a low-gravity environment. Reported here are the first demonstrations of LII performed in a low-gravity environment provided by the NASA-Lewis 2.2 sec drop tower facility. Examples shown include laminar gas-jet diffusion flames of acetylene/nitrogen, ethane, a turbulent gas-jet diffusion flame of acetylene and vortex formed by a transient propane gas-jet flame.

Experimental

Experiments were performed in the 2.2 sec drop tower facility at NASA-Lewis. Experiments are contained within packages measuring 16×33×38 in. (W×L×H) with maximum weight of 350 lb. Release of the package into free-fall yields a low-gravity duration of ~2.2 sec during which peak accelerations of $\sim 10^{-4}$ g are experienced. Peak decelerations of 15 to 30 g occur during 0.2 sec. A detailed description is available elsewhere [19].

To enable LII, light from a pulsed Nd:YAG laser was delivered via a 35 m long section of high OH-content, 1000 μm core diameter (30 μm cladding thickness) optical fiber to the drop package from the laser resident on the top floor of the drop tower. The jacket of the optical fiber consisted of black PVC with Kevlar-strengthening fibers. A special high power SMA-905 input connector was vital to coupling of the pulsed laser light into the optical fiber. Laser light at 532 nm from a short cavity, pulsed Nd:YAG laser manufactured by Big Sky Laser Inc., was coupled into the optical fiber using a 200 mm focal length plano-convex BK-7 lens. The combined coupling efficiency of laser light into plus transmission through the 35 m optical fiber was roughly 75%.

Figures 1(a) and (b) illustrate top and side views of the drop rig layout respectively. The divergence of the laser light at 532 nm emerging from the optical fiber is reduced by a 50-mm diameter, 100-mm-focal-length fused silica spherical lens placed ~40 mm after the fiber. A sheet is formed using a 125-mm focal length, 50-mm round cylindrical lens. Only the central 30 mm of the light sheet, representing the most uniform intensity, is used for creating the LII images detected by the intensified gated array camera. A dichroic mirror following the cylindrical lens allowed for precise placement of the light sheet through the flame centerline. A beam dump collected the laser light after the burner thereby eliminating scattered laser light. With an incident energy of 10 mJ and estimated beam sheet width of 400 μm, the laser intensity was roughly 1×10^7 W/cm^2.

LII images were detected by a ruggedized Xybion ISG-250 ICCD camera through a bandpass interference filter transmitting 400-450 nm. A glass lens used at f/8 fitted with a 10 mm extension tube provided a field-of-view of 30 mm. A custom electronics module provided power to the camera from the rig batteries and coupled the video and related timing signals out from the ICCD camera and gate pulse into the camera intensifier. Natural flame luminosity was detected by a Sony XC-77 black and white camera or a Sony XC-999 color video camera.

Figure 2 illustrates the equipment and signals layout. Video signals from both cameras were transmitted though FM (6 MHz bandwidth) video transmitters attached to the drop rig, a dual fiber-optic video cable running between the drop rig and FM video receivers located on the top floor of the drop tower. The LII signal was recorded on a Beta video tape while the natural flame luminosity was recorded on SVHS video tape. Synchronization of the laser, camera intensifier gate and camera video signal was achieved using custom electronics to detect the top-of-frame pulse on each video frame and provide a trigger pulse to a delay generator. The delay generator in turn triggered the laser and provided an inverted TTL pulse to serve as the gate pulse for the ICCD camera intensifier. The pulse was delivered through a 35 m length of BNC (RG58) cable connected to the camera control unit aboard the drop rig. A frame-grabber digitized data for subsequent analysis.

Drops were initiated by loading a computer program into an onboard data acquisition/control system. This unit also controlled solid state relays to deliver power to the spark ignitor, cameras, and gas solenoid. A preburn prior to the drop ensured fuel within the gas-jet nozzle and confirmation of all systems working. Upon package release into free-fall, an electrical circuit was opened to provide a rising edge TTL trigger to initiate fuel delivery and ignition.

Comparison of pixel intensities between the LII images of the preburn (in 1-g) and those in 0-g allow assessment of the relative changes in f_v. Spatial locations within the flames for these comparisons are indicated in the results section. A calibration of the digitized LII intensity with camera intensifier gain was performed in 1-g using the complete system for laser light delivery, image detection, video recording and subsequent digitization. This calibration provides a means of relating LII intensities of different flame systems to a reference flame system with known f_v previously determined via light extinction [20].

Laminar gas-jet diffusion flames were established on a 1.1 mm i.d. Nozzle with approximately a 30° outside edge taper. The burner for the turbulent gas-jet diffusion flame utilized a 0.51 mm i.d. nozzle (length/diameter >20) with a coannular pilot diffusion flame. In each case a regulator and fine control valve were adjusted against a mass flow meter to deliver a known fuel flow rate. The acetylene flow through the central gas-jet tube was 1.0 slpm giving a Reynolds number of 4250 while the acetylene flow for the laminar coannular pilot flame was roughly 10 sccm.

Results and Discussion

LII System Response

Figure 3 illustrates the measured system dependence upon LII intensity. To test this dependence, a laminar steady-state gas-jet flame of ethylene was established in 1-g supported on the same 1.1 mm I.D. burner nozzle with a fuel flow rate of 48 sccm. The signal excitation and detection were setup as if the measurements were being performed in low-gravity. Consequently, the graph represents the results of an end-to-end test of the LII signal detection, transmitting and processing equipment which includes the

intensified camera, the video fiber-optic transmitter plus receiver, beta recorder and the frame-grabber used for digitization of the video signal. With a fixed camera intensifier gain typical of that needed for LII 0-g measurements, the LII intensity reaching the camera was varied by placing calibrated neutral density filters in the detection optical path. Within the resulting digitized LII image, a region-of-interest (ROI) was defined containing 624 pixels within the flame tip where a rather spatially uniform fv distribution (less than 20% spatial intensity variation) was observed. The average pixel intensity within this region was then calculated. Since the LII intensity incident upon the camera photocathode varied as,

$$\text{Signal}_{(\text{det.})} = C * LII * 10^{(-\text{N.D.})}$$

where C is a constant, a semi-logarithmic plot of $\text{Signal}_{(\text{det.})}$ versus N.D. filter value should be linear provided all subsequent signal processing is linearly dependent upon the LII signal. This is observed in Fig. 3. The error bars represent one standard deviation of the ROI average intensity. Even if the curve were nonlinear, it would still provide a calibration curve for translating final digitized pixel intensities into relative LII intensities. The observed linearity allows straightforward interpretation of LII intensities as proportional to f_v.

Camera gain calibration

Lower LII signals arising from lower soot concentrations could be readily detected by increasing the camera intensifier gain. To establish the relative detection sensitivities at different intensifier gains, calibration measurements were performed. Again, the entire LII excitation/detection system was set up as if to perform low-gravity measurements. LII images of a laminar steady-state flame of ethylene (48 sccm flow rate) were acquired using different intensifier gains. Neutral density filters maintained the signal intensity within the dynamic range of the detection system. Analysis of a ROI (620 pixels) near the tip of the flame provided an average LII intensity for the particular gain setting. Comparison of the relative LII intensities corrected for the neutral density filter attenuation provided a relative measure of the detection sensitivity at the different gain settings (higher intensifier gains correspond to smaller readout values). To facilitate comparison, the relative values were normalized by the LII average intensity measured with the lowest practical gain setting. These results are shown in Fig. 4. The error bars were calculated assuming Poisson statistics with the standard deviation calculated as the square root of the average LII pixel intensity. These limits were found empirically to well encompass the variation observed in the average LII intensity calculated within the ROI.

Although the semi-logarithmic plot conveniently illustrates the range of detection sensitivities, there is a physical basis for this method of plotting. Because the photon detection event is described by a Poisson distribution [20] and the intensifier amplification process is exponential [21], with a linear detection system, the detected signal intensity would be expected to scale exponentially with the intensifier gain provided no saturation of the electron multiplication process occurred within the microchannel plate, coupled phosphor screen or CCD pixel well. As Fig. 4 shows, using the intensifier, more than a 1000-fold increase in detection sensitivity can be achieved relative to that at a gain setting of 4.70. Based on soot volume fractions of about 15 ppm for a laminar acetylene/nitrogen mixture in 1-g detected using a gain of 4.70, Fig. 3 predicts a detection sensitivity of nearly 0.01 ppm.

Validation of LII

To verify the validity of the LII measurements as representative of f_v, LII radial intensity profiles are compared with those derived from a full-field extinction method for a laminar gas-jet flame of 50/50 nitrogen/acetylene (volume/volume). The light extinction results have been reported previously [22]. The axial positions were chosen to illustrate different spatial and intensity variations in f_v and are indicated in Fig. 5. Three radial pixel rows of the LII image were averaged together for better signal-to-noise thus giving a spatial resolution of 0.25 mm. Each LII profile was also corrected for attenuation by soot between the LII image plane and camera. To convert the relative LII intensities to f_v, each LII radial profile was multiplied by a scaling factor which was determined by the ratio of the summed LII intensity from all three radial profiles to the radially summed f_vs from all three axial positions. As can be seen from Fig. 5, good agreement is observed between the LII measurements and those derived from extinction where both the relative spatial variations and intensities are similar. While previous tests of LII have shown it to yield accurate relative measurements in 1-g by comparison with light extinction and gravimetric sampling, these results are the first tests validating LII as a diagnostic for f_v in 0-g.

Additional Demonstrations

Laminar gas-jet flame

Figure 6 shows LII images obtained from a gas-jet diffusion flame in 1-g and 0-g. In each case, the ethane fuel flow rate was 70 sccm with resulting Reynolds number of 200. Due to buoyancy-induced instabilities, the normal gravity flame frequently flickered, consequently a representative image was chosen. As clearly seen in Fig. 6(a), buoyant acceleration overcomes the divergent cold-gas flow causing radial confinement of the flame. With soot oxidation proceeding inward towards the flame centerline, soot on the jet

centerline is oxidized last resulting in the steeple shaped soot distribution at the flame tip. With buoyant acceleration eliminated in 0-g, the initial divergence of the exiting fuel flow is largely preserved resulting in a flame spatial extent determined much more by stoichiometric requirements than in 1-g. Similar to the laminar gas-jet flame of the 50/50 nitrogen/acetylene mixture, absence of buoyant entrainment leads to an increase in the spatial extent of soot inception and growth. Despite the fuel abundance within the central core of the flame, a combination of insufficient fuel pyrolysis products and diminished temperatures relative to 1-g likely inhibit soot formation reactions along the axial streamline resulting in the absence of soot at the flame tip.

Although the flicker observed in 1-g causes variation in peak f_v (ranging from 0.3 to 0.6 ppm in the tip of the flame), the ratio of the 0-g to 1-g f_v is roughly 3 based on a comparison of LII intensities. This example also illustrates the sensitivity of LII as the radially integrated f_v-pathlength product is 6.7×10^{-7} cm yielding a transmittance of 0.95 using Ke = 4.9 from Dazell and Sarofim [25]. Such a high transmittance is marginally detectable using unstabilized HeNe lasers and biased photodetectors and 8-bit digitization. On the basis of the camera gain calibration curve, approximately a factor of 30 higher sensitivity (or a factor of 30 lower f_v) is achievable using a camera gain of 4.40 compared to 4.575 as was presently used. Such a high transmittance is likely undetectable even using sensitive lock-in detection of absorbance which possesses a practical limit of roughly 0.1% absorbance sensitivity with RC timeconstants on the order of 100's of msec.

Turbulent gas-jet flame

Figure 7(a), perhaps the best illustration of the temporal plus spatial capabilities of LII and its geometric versatility, shows a LII image from a turbulent acetylene gas-jet flame in 0-g with Reynolds number of 4250. Figure 7(b) is a contour plot of Fig. 7(a). Absolute soot volume fractions were calculated based on the LII image intensity in the turbulent flame relative to that of the reference flame system using the camera intensifier calibration curve of Fig. 4. Even using a detection gate of 500 ns to ensure capture of the LII signal, temporal frequencies of greater than 1 MHz can be frozen. As determined using a replica of the 1951 Air Force test pattern, the spatial resolution is ~5 line pairs/mm allowing spatial structures of 0.1 mm to be resolved.

Vortex visualization

Figure 8(a) is a LII image of soot within a vortex formed by propane fuel issuing from a gas-jet nozzle while Fig. 8(b) is a contour plot of Fig. 8(a). Based on the relative pixel intensities and camera gain calibration curve, absolute f_vs were assigned to the intensity contours derived from Fig. 8(a). The central bulge is due to the initial jet momentum while the side recirculation regions result from air entrainment into the shear layer. Initiation of fuel flow and subsequent ignition were performed in low-gravity (after package release from the "music" wire). The nominal jet Reynold's number was 330 based on the nozzle ID of 1.1 mm and flow rate of 70 sccm. The higher f_v in the recirculation regions is sensible as fuel parcels in these regions experience extended times at elevated temperatures promoting pyrolysis processes and soot growth. Visualization of the transient vortex and resolution of the steep spatial gradients requires the temporal and spatial capabilities of LII.

Conclusions

Combustion processes exhibit rather different features in microgravity compared to normal gravity. With the elimination of buoyancy-induced convection, both flame shape and f_v differ substantially compared to the same fuel/burner system in normal gravity. The sensitivity, temporal and spatial capabilities in addition to geometric versatility enable LII to reveal the soot volume fraction regardless of these differences. Validation of LII for f_v determination in 0-g was demonstrated by comparison of LII radial intensity profiles with radial f_vs derived via extinction for a laminar gas-jet flame of acetylene/nitrogen in 0-g. Application of LII to a laminar gas-jet diffusion flame of ethane demonstrates the high sensitivity of LII. Imaging of f_v in a turbulent gas-jet diffusion flame of acetylene and vortex formed by a transient propane gas-jet flame illustrate the high temporal and spatial capabilities of LII. Spatial and concentration differences of f_v in 1-g and 0-g environments is readily illustrated by comparison of the LII images.

Disclaimer

Manufacturer and product names are used to aid understanding and do not constitute an endorsement by the federal government.

Acknowledgements

This work was supported through NASA contract, NAS3-27186. The author thanks Prof. J. C. Ku (Wayne State University) and P. S. Greenberg (NASA-Lewis) for sharing their full-field light extinction data.

References

1. Echigo, R., Nishiwaki, N. And Hirata, M., The Eleventh Symposium on Combustion (International), The Combustion Institute, (1976) p. 381.
2. Gore, J. P. And Faeth, G. M., J. Heat Transf. 110:17 (1988).
3. Bahadori, M.Y., Edelman, R.B., Stocker, D.P. and Olson, S.L., AIAA J. 28:236 (1988).
4. Pitts, W.M., Prog. Energy Combust. Sci. 21:197 (1995).

5. Ross, H.D., Prog. Energy Combust. Sci. 20:17 (1994).
6. Bockhorn, H., Hornung, A., Hornung, U., Teepe, S. And Weichmann, J. Combust. Sci. and Technol. 116-117:129 (1997).
7. Proceedings of the Third International Microgravity Combustion Workshop, (NASA CP-10174), April 11-13, Cleveland, OH (1995).
8. Dec, J.E., zur Loye, A.O. and Siebers, D.L., SAE TP-910224 (Society of Automotive Engineers), Warrensdale, PA, (1991).
9. Pinson, J.A., Mitchell, D.L., Santoro, R.J. and Litzinger, T.A., SAE TP-32650 (Society of Automotive Engineers), Warrensdale, PA, (1993).
10. Quay, B., Lee, T.W., Ni,T. and Santoro, R.J., Combust. and Flame 97:394 (1994).
11. Vander Wal, R.L. and Weiland, K.J., J. Appl. Phys. B59:445 (1994).
12. Shaddix, C.E., Harrington, J.E. and Smyth, K.C., Combust. and Flame 99:723 (1995).
13. Shaddix, C.R. and Smyth, K.C., Combust. and Flame 107:418-452 (1996).
14. Ni, T., Pinson, J.A., Gupta, S. and Santoro, R. J., Appl. Opt. 34:7083 (1995).
15. Vander Wal, R.L., Jensen, K.A. and Choi, M.Y., Combust. and Flame (in press).
16. Vander Wal, R.L. Combust. Sci. and Technol. 118:343-360 (1996).
17. Vander Wal, R.L., Zhou, Z. and Choi, M.Y., Combust. And Flame 105:462 (1996).
18. Vander Wal, R.L. and Dietrich, D.L., Appl. Opt. 34:1103 (1995).
19. Lekan, J., Gotti, D.J., Jenkins, A. J., Owens, J.C. And Johnston, M.R., NASA TM-107090, April, (1996).
20. Stanford Research Systems, Application Notes, 1996-1997, Note no. 4, p. 186.
21. Engstrom, R.W., RCA Photomultplier handbook, The RCA Corporation, (1980).
22. Greenberg, P.S. and Ku, J.C., Combust. And Flame 108:227 (1997).

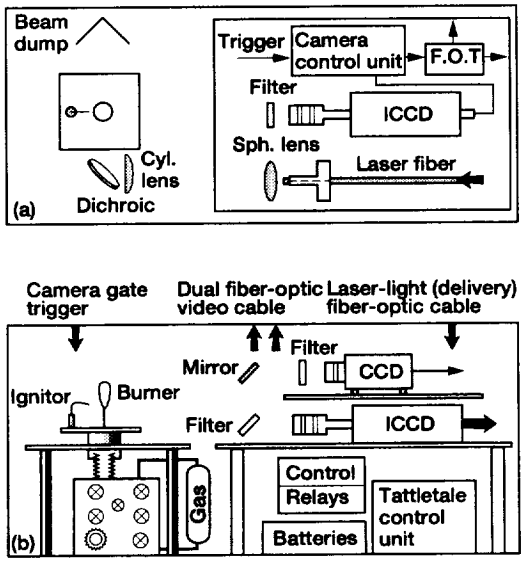

Figure 1.—(a) Top view of the hardware and optical layout of the drop rig. (b) Corresponding side view.

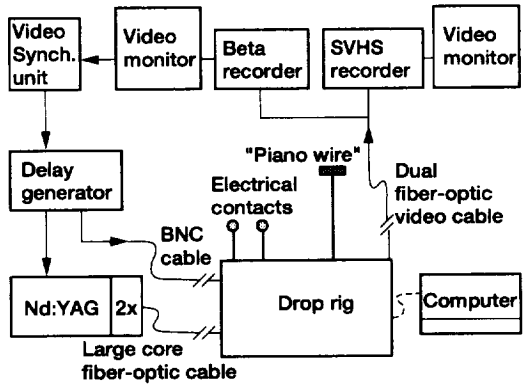

Figure 2.—Equipment and signals layout.

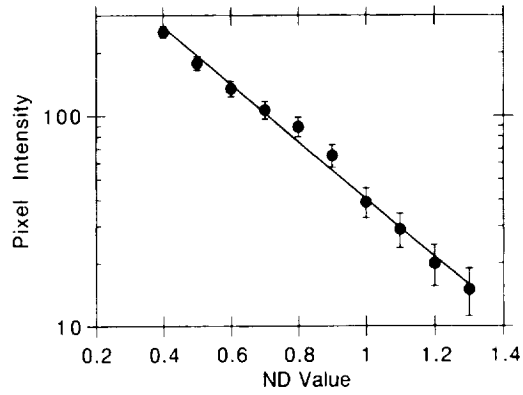

Figure 3.—Average LII pixel intensity versus neutral density filter value (ND) preceding the LII camera. See text for details.

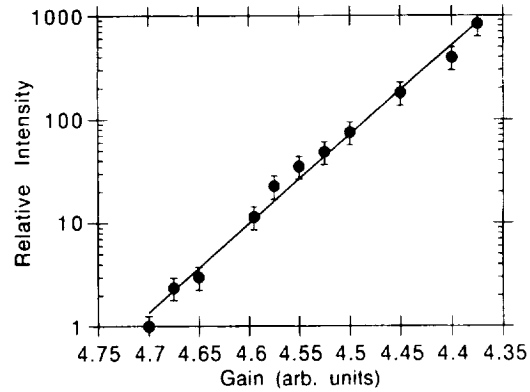

Figure 4.—Camera intensifier gain calibration curve. Note that higher intensifier gains correspond to smaller values of the gain setting.

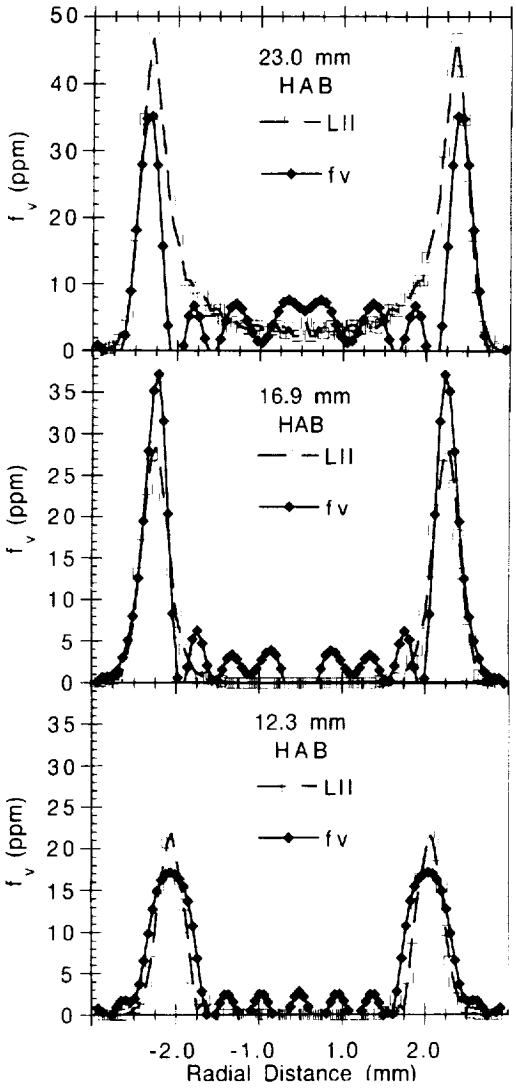

Figure 5.—Radial intensity profiles for a 50/50 acetylent/nitrogen (volume/volume laminar gas-jet flame in both 1-g and 0-g. Comparison is made between the LII signal instensity and f_v values derived from a full-field light extinction method discussed elsewhere (ref. 22). See text for details.

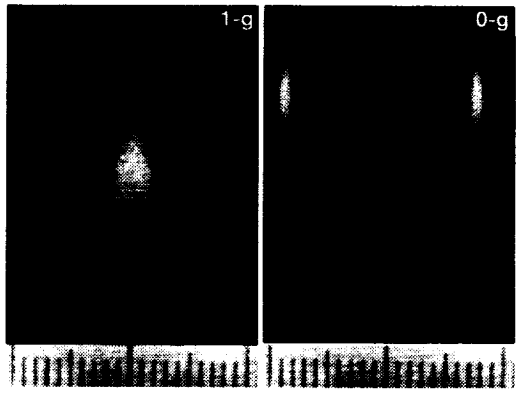

Figure 6.—LII images of a laminar ethane gas-jet diffusion flame in 1-g and 0-g. The burner nozzle is 11 mm below the picture bottom (but not observable in the LII image). Ruler spatial scale is in mm.

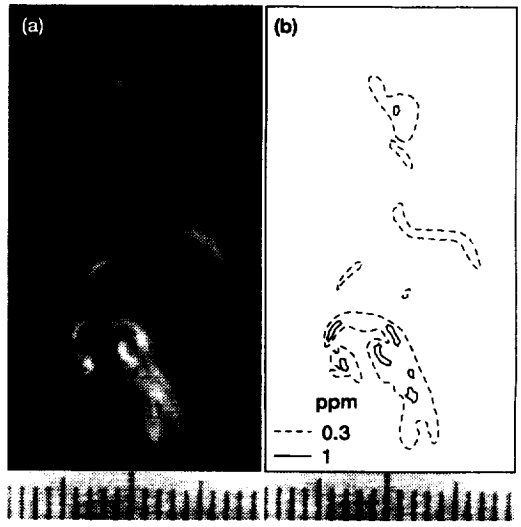

Figure 7.—(a) LII image of soot within the oxidation region of a turbulent gas-jet flame of acetylene. (b) Contour plot of (a) with f_v values given in ppm. The image bottom is 100 mm above the burner nozzle. The ruler spatial scale is in mm.

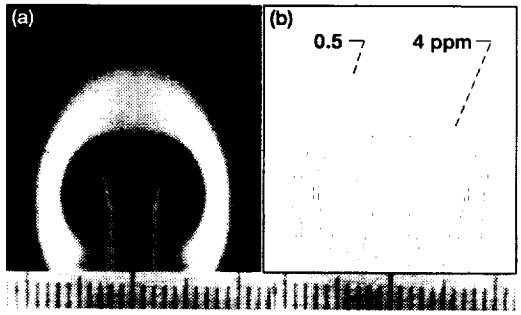

Figure 8.—(a) LII image of a vortex formed during initial formation of a laminar gas-jet flame of propane in 0-g. (b) Contour plot of (a) with f_v values given in ppm. Both fuel flow and ignition were initiated in 0-g. The nominal steady-state fuel flow rate was 70 sccm. The burner nozzle is 11 mm below the picture bottom (but not observable in the LII image). The ruler spatial scale is in mm.

REPORT DOCUMENTATION PAGE

Form Approved
OMB No. 0704-0188

1. AGENCY USE ONLY (*Leave blank*)	2. REPORT DATE	3. REPORT TYPE AND DATES COVERED
	May 1997	Final Contractor Report

4. TITLE AND SUBTITLE

Characterization and Demonstrations of Laser-Induced Incandescence in Both Normal and Low-Gravity

5. FUNDING NUMBERS

WU–963–70–0E
C–NAS3–27186

6. AUTHOR(S)

Randall L. Vander Wal

7. PERFORMING ORGANIZATION NAME(S) AND ADDRESS(ES)

NYMA, Inc.
2001 Aerospace Parkway
Brook Park, Ohio 44142

8. PERFORMING ORGANIZATION REPORT NUMBER

E–10683

9. SPONSORING/MONITORING AGENCY NAME(S) AND ADDRESS(ES)

National Aeronautics and Space Administration
Lewis Research Center
Cleveland, Ohio 44135–3191

10. SPONSORING/MONITORING AGENCY REPORT NUMBER

NASA CR–202347

11. SUPPLEMENTARY NOTES

Prepared for the Central States Section Meeting sponsored by the Combustion Institute, Point Clear, Alabama, April 27–29, 1997. Project Manager, Howard D. Ross, Space Experiments Division, NASA Lewis Research Center, organization code 6711, (216) 433–2562.

12a. DISTRIBUTION/AVAILABILITY STATEMENT

Unclassified - Unlimited
Subject Category 25

This publication is available from the NASA Center for AeroSpace Information, (301) 621–0390.

12b. DISTRIBUTION CODE

13. ABSTRACT ***(Maximum 200 words)***

Knowledge of soot volume fraction is important to a wide range of combustion studies in microgravity. Laser-induced incandescence (LII) offers high sensitivity, high temporal and spatial resolution in addition to geometric versatility for real-time determination of soot volume fraction. Implementation of LII into the 2.2 sec drop tower at The NASA-Lewis Research Center along with system characterization is described. Absolute soot volume fraction measurements are presented for laminar and turbulent gas-jet flames in microgravity to illustrate the capabilities of LII in microgravity. Comparison between LII radial intensity profiles with soot volume fraction profiles determined through a full-field light extinction technique are also reported validating the accuracy of LII for soot volume fraction measurements in a microgravity environment.

14. SUBJECT TERMS

Soot; LII; Laser-induced incandescence; Microgravity

15. NUMBER OF PAGES

8

16. PRICE CODE

A02

17. SECURITY CLASSIFICATION OF REPORT	18. SECURITY CLASSIFICATION OF THIS PAGE	19. SECURITY CLASSIFICATION OF ABSTRACT	20. LIMITATION OF ABSTRACT
Unclassified	Unclassified	Unclassified	